Experimental Observations on the Influence of Hydrogen Atoms Diffusion on Laminar and Turbulent Premixed Burning Velocities

A.A. Burluka[a], R.G. Gaughan[b], J.F. Griffiths[c], C. Mandilas[a,*], C.G.W. Sheppard[a], R. Woolley[d]

[a] School of Mechanical Engineering, The University of Leeds, Leeds LS2 9JT, UK

[b] ExxonMobil Research and Engineering Company, Paulsboro Technical Center, 600 Billingsport Road, Paulsboro, NJ 08066, USA

[c] School of Chemistry, The University of Leeds, Leeds, LS2 9JT, UK

[d] The University of Sheffield, Department of Mechanical Engineering, Mappin Street, S1 3JD, UK

[*] Corresponding author. Present address: The Centre for Research and Technology, Hellas, Chemical Process & Energy Resources Institute, 3km Charilaou-Thermi Road, Thermi 57001, Greece, mandilas@cperi.certh.gr

Abstract

Measurements of the laminar and turbulent burning velocity of premixed hydrogen – air, n-hexane – air and n-octane – air flames were made and compared to corresponding measurements of deuterium – air, n-hexane-d14 – air and n-octane-d18 – air flames performed at identical initial conditions. Experiments were conducted in a constant volume, optically accessed vessel, at elevated initial pressure and temperature of 0.5 MPa and 360 K, for a range of equivalence ratios. Burn rate data was determined via schlieren imaging of flames. It was found that the isotope effect accounted for an average reduction of 20% in the laminar burn rate of alkanes. Similarly, deuterium was measured to burn around 30% slower than hydrogen at the range of equivalence ratios explored. The isotope effect on burn rate was significantly reduced under turbulence. The difference between the turbulent burn rates of the deuterated alkanes and their normal alkane counterparts were measured to be approximately 10%. The difference between the turbulent burn rates of deuterium and hydrogen was even smaller. Nonetheless, the laminar burn rate ranking was maintained under turbulence for all fuels and conditions explored, thus suggesting a degree of influence of radical transport and chemistry under turbulent burning.

Keywords: laminar flames, turbulent flames, burning velocity, hydrogen combustion, deuterium combustion, isotope effect

Nomenclature

Latin Symbols

D	m^2/s	Mass diffusivity
k	$m^3/mol.s$	Reaction rate coefficient

44	L	m	Integral length scale of turbulence
45	L_b	m	Burnt Markstein length
46	P_i	Pa	Initial pressure
47	r_u	m	Cold flame mean flame radius
48	T_{ad}	K	Adiabatic flame temperature
49	T_i	K	Initial temperature
50	S	-	Laminar burning velocity sensitivity factor
51	u'	m/s	Turbulent root-mean-square velocity
52	u_l	m/s	Unstretched, one-dimensional laminar burning velocity
53	u_n	m/s	Stretched, entrainment laminar burning velocity
54	u_{te}	m/s	Entrainment turbulent burning velocity
55			
56	Greek Symbols		
57	α	m^2/s	Thermal diffusivity
58	α_{mix}	m^2/s	Thermal diffusivity of mixture
59	α	1/s	Flame stretch rate
60	δ_l	m	Laminar flame thickness
61	η	m	Kolmogorov length scale of turbulence
62	ϕ	-	Equivalence ratio
63	ω	$(m^3/mol.s)^n$	Global reaction rate
64			

1. Introduction

The molecular structure of a fuel (i.e. length of chain, branching, bonding) is known to greatly influence the laminar burn rate [1-5]. Fuel structure in conjunction with mixture stoichiometry, pressure and temperature, govern the thermodynamics and chemical kinetics of combustion. One of the main driving forces of chemical kinetic contributions to the control of burning velocity is the radical pool at the flame front, with H atoms being the most important by virtue of their extremely high diffusivity and reactivity [4-5].

In two previous papers we investigated the effects of fuel structure on the laminar and turbulent burning velocities of gasoline components. We assessed:

(i) isomeric structure and bonding through experimental studies of seven different hydrocarbons containing six carbon atoms, over a wide range of fuel - air mixtures [6] and

(ii) chain length and molecular mass by reference to straight chain alkanes in the range C_5 – C_8 [7].

Interpretation of the results was linked to the influence of H radicals at the flame front in controlling the burn rate.

The object of the present work was to understand the importance of the transport and kinetic effects of hydrogen radicals within laminar and turbulent premixed flames via experimental studies of burning velocity measurements of freely propagating flames. Hence, we have extended the earlier studies [6, 7] through comparisons of laminar and turbulent velocity of n-hexane and n-octane (i.e. n-C_6H_{14} and n-C_8H_{18}) with those of their fully deuterated forms (i.e. n-C_6D_{14} and n-C_8D_{18}). In interpretation of the results, it is assumed that there are no qualitative differences in the kinetic mechanisms involved in flame propagation of the normal and deuterated fuels. In

addition, we explore the H / D isotopic effect in its most influential guise, via an investigation of the laminar and turbulent burning velocities of H_2 and D_2.

The available literature on the isotopomoric effects in combustion is sparse. With the exception of a study of laminar flame propagation in acetylene and di-deuteroacetylene by Friedman and Burke [8], we are not aware of any other investigation of the laminar and turbulent burn rates of deuterated versus normal hydrocarbons, even though the former are occasionally used for tracing the origins of pollutants in flames, e.g. [9]. Moreover, although hydrogen burn rate data exist for a variety of conditions [e.g. 10-18] there is only very little information on the laminar burn rates of D_2 [19-21] and, to our knowledge, no comparisons between the turbulent burn rates of H_2-air and D_2-air flames.

2. Experimental Apparatus and Data Processing

All measurements were performed in the Leeds MkII spherical bomb [22]. As in the previous studies for the examination of fuel structure and chain length effects on burn rate [6-7], measurements were performed at elevated temperature and pressure (360 K and 0.5 MPa), at which the premixed turbulent flames demonstrate behaviour similar to flames in spark-ignition engines [22]. Owing to the high cost of the deuterated fuels, the alkane tests were undertaken at only $\phi = 0.8$ and $\phi = 1.0$ for laminar conditions and at $\phi = 1.0$ under turbulent conditions. For the latter, the turbulence level was set at an rms velocity of u' = 4 m/s. The burn rates of H_2 and D_2 were examined for laminar and turbulent (u' = 4 m/s) conditions for $0.6 \leq \phi \leq 1.1$. The turbulence rms velocity of u' = 4 m/s chosen for this study was relevant to reciprocating engines, where u' near the top dead centre is about half the piston speed (e.g. u' = 5 m/s, for 75 mm stroke, at 4000 rpm [23]).

Premixed mixtures were prepared inside the fan-stirred vessel. Pre-calculated volumes of liquid fuels were injected into the vessel under vacuum conditions, using a gas tight syringe. For gaseous fuels, the mixture stoichiometry was controlled by measuring the partial pressure of the fuel injected into the bomb at atmospheric pressure. The bomb fans were continuously operated during mixture preparation to ensure full mixing and to assist heat transfer from the 2 kW electrical heater, positioned close to the walls of the vessel. For laminar studies, the fans were switched off for a period of 60 seconds, following mixture preparation, and before ignition. For turbulent studies the fans were maintained at the speed required to produce the desired rms turbulent velocity throughout the mixture preparation, ignition and combustion period. The pressure in the vessel before ignition was measured via an absolute pressure transducer (Druck PDCR-911) with a range of 0 to 0.7 MPa. Following spark discharge, the pressure rise in the vessel was monitored with a Kistler-701 piezoelectric pressure transducer, flush mounted on the side of the vessel. After each experiment the vessel was flushed several times with compressed air and then evacuated. Dry cylinder air was provided for the combustible mixture.

At least two laminar and five turbulent deflagrations were performed at each condition. Centrally ignited advancing flames were imaged via the schlieren method to the bomb window diameter of 150 mm, using a Photosonics Phantom Series 9 high speed digital camera. Laminar flames were recorded at 4000 frames/s with a resolution of 576x576 pixels. Turbulent flames were photographed at a rate of 9000 frames/s with a resolution of 384x384 pixels.

During post-processing of schlieren data, each flame image was converted from grayscale to black and white. White corresponded to the burned and black to the unburned region. The flame area was found by counting the number of white pixels. The burning velocity was then defined as the radius derivative with respect to time divided by the ratio of densities of the fresh mixture to

that of the combustion products. Mean flame radius was determined as that of a circle encompassing the same area. Further information on the flame image processing procedure is given in [6, 24]. Imaging data analysis to obtain laminar flame characteristics (burning velocity, stretch rate and Markstein lengths) and turbulent burn rates followed established methods, detailed [25-26] and widely used elsewhere [eg. 27-31].

3. Results

Presented in this section are measured laminar and turbulent burn rate results for normal and deuterated alkanes, hydrogen and deuterium. Experimental scatter for laminar deflagrations was at a maximum of 2% with respect to the coefficient of variance (COV) of the laminar burning velocity at any given flame radius. Turbulent deflagrations reported here exhibited an average scatter of circa 7-8% in COV of the turbulent burn rate at a given flame radius, which was similar to that reported in [32] and is typical of the magnitude of cycle-to-cycle variation of the burning rate in an SI engine [33].

In addition to data for the unstretched, one dimensional, laminar burning velocity, u_l, derived in accord with [26], the laminar results for the alkanes also include data for the stretched laminar burning velocities, u_n, at mean flame radii of 10 mm and 30 mm. Due to the comparable molar mass of n-hexane versus n-hexane-d14 and n-octane versus n-octane-d18, stretch rate effects were anticipated to be similar and, therefore, to not affect the trends observed for the laminar burn rate ratio of normal vs deuterated alkanes.

For H_2 and D_2 laminar deflagrations, hydrodynamic flame instabilities [34-35] occurred too early to apply the criteria for unstretched laminar burning velocity [26]. It was thus decided to present

155 the schlieren-derived stretched burning velocities at mean flame radii of 10 mm and 30 mm to
156 allow comparison to previous studies [13] and ensure exclusion of spark effects [36].
157 All schlieren based turbulent burn rates, u_{te}, refer to a mean flame radius of 30 mm. Reasons
158 behind this choice are discussed in [6]. As a brief recapitulation here, presentation of the
159 turbulent burn rate results at this radius offered the best compromise between ensuring that the
160 flame had experienced most (~ 62% [25]) of the effective turbulence [37] inside the vessel, while
161 also avoiding extra difficulties during image processing induced due to flame convection from
162 the centre of the visible area of the vessel, which is a particular problem for lean, high turbulence
163 flames [24].
164
165 **3.1 Laminar Burning Velocities of the Alkanes**
166 The development of spherical expanding flames of normal and deuterated hexane and octane is
167 depicted via the sequences of schlieren images displayed in Figure 1 for $\phi = 0.8$ and Figure 2 for
168 $\phi = 1.0$. Starting at mean flame radii of 30 mm, the images of each of the flame filmstrips are in
169 steps of 10 ± 0.2 mm in mean flame radius. Also shown below each image is the time elapsed
170 from the first visible flame kernel following ignition. Although lean flames did not exhibit
171 transition to fully cellular structure within the field of view of the bomb windows, the formation
172 of large scale cells on the flame surface was more apparent for the normal than for the deuterated
173 alkanes at radii of 60 ± 0.2 mm. Flames at stoichiometric conditions became fully cellular at ca.
174 45 mm for the normal alkanes and at ca. 50 mm for the deuterated alkanes. This is linked to
175 differences in the thermo-diffusive properties at the flame front [35, 38], which in this case have
176 been induced solely by the isotope effect. Note that the definition of the onset of cellularity was
177 based on photographic observations for the formation of small scale cells at the flame surface

(Figures 1 and 2) in conjunction with identification of the point at which an appreciable flame acceleration appears on the plot of burning velocity vs. mean flame radius, as described in [7, 35].

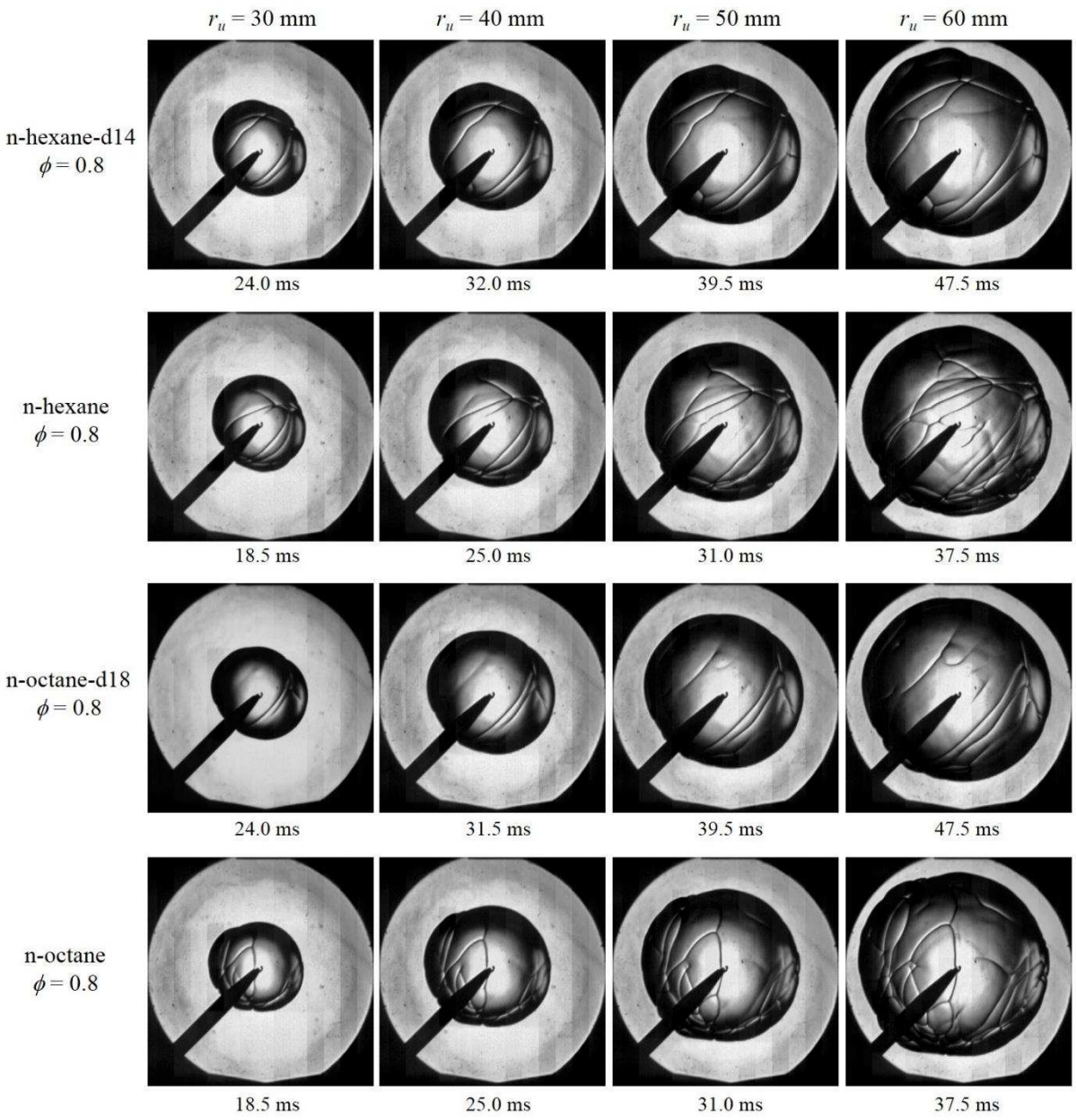

Figure 1 – Filmstrip (left to right) of schlieren images showing the flame development for normal and deuterated alkane flames of ϕ = 0.8. The mean flame radius values indicated have an accuracy of ± 0.2 mm, while the time values shown in milliseconds represent time elapsed from the first visible flame kernel following ignition.

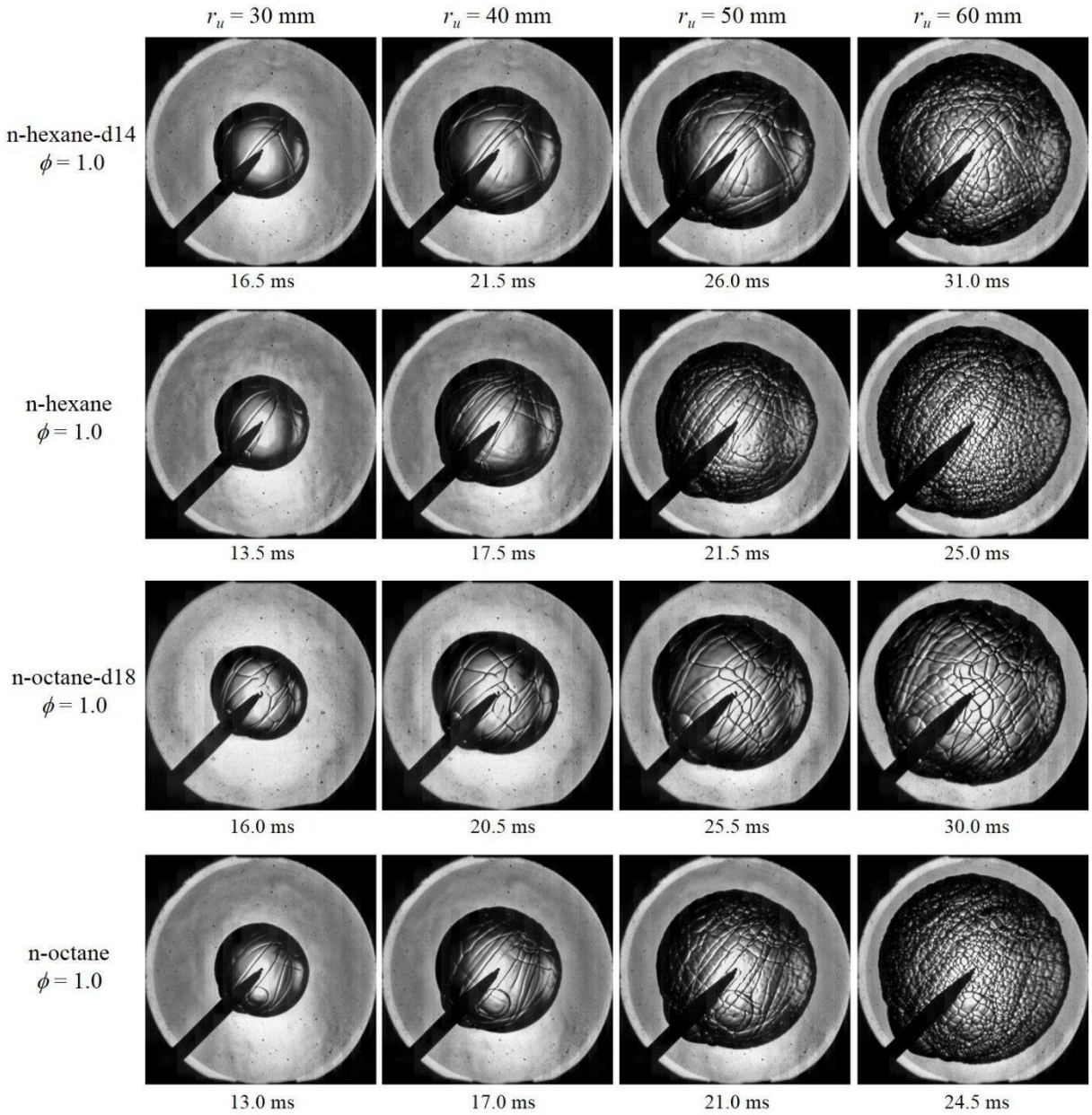

Figure 2 – Filmstrip (left to right) of schlieren images showing the flame development for normal and deuterated alkane flames of ϕ = 1.0. The mean flame radius values indicated have an accuracy of ± 0.2 mm, while the time values shown in milliseconds represent time elapsed from the first visible flame kernel following ignition.

The onset of apparent transition to fully cellular flames is specified on the u_n vs r_u plots of Figure 3 via the red asterisk symbols on top of the data points. Also specified on these plots is the early flame development region affected by the characteristics of the igniter. Spark energy much above the minimum ignition energy, can cause a very high initial flame speed due to the expansion of the plasma and the conductive energy transfer from it; these data are disregarded [26]. Previous measurements in the same apparatus have shown the spark affected area to be up to a mean flame radius of 8-10 mm [36]. For lean flames the slight increase in burning velocity with radius is attributed to the reduction of stretch rate with flame radius, as well as to a small increase of ~10 K in unburned gas temperature over that period of flame development [24]. Stoichiometric flames exhibited similar behaviour up to the point of transition to fully cellular regime, upon which a slight increase in flame acceleration was observed, for reasons described in [7]. For completion, the variation of burning velocity with stretch rate (α) is shown in Figure 4, along with the range of data over which the laminar flame theory described in [26] was applied to determine the true laminar, one-dimensional and unstretched burning velocities, u_l.

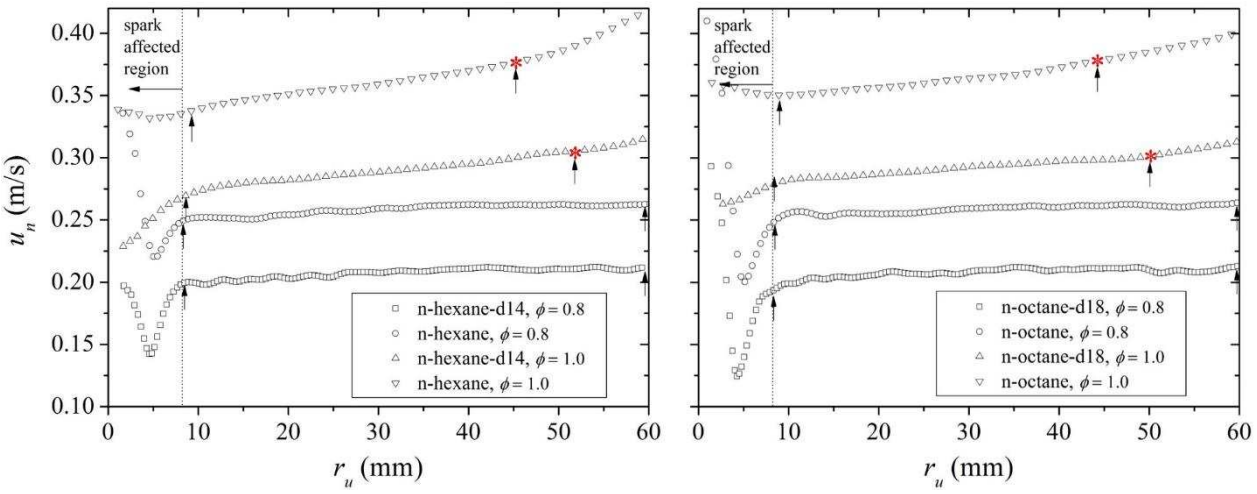

209

210 Figure 3 – Stretched burning velocity, u_n, plotted against mean flame radius, r_u, for normal and
211 deuterated alkanes at ϕ = 0.8 and 1.0. Vertical arrows indicate the data regions used for
212 application of laminar burn rate theory to obtain unstretched burning velocity and Markstein
213 lengths. The red asterisks indicate the onset of transition to fully cellular regime.

214

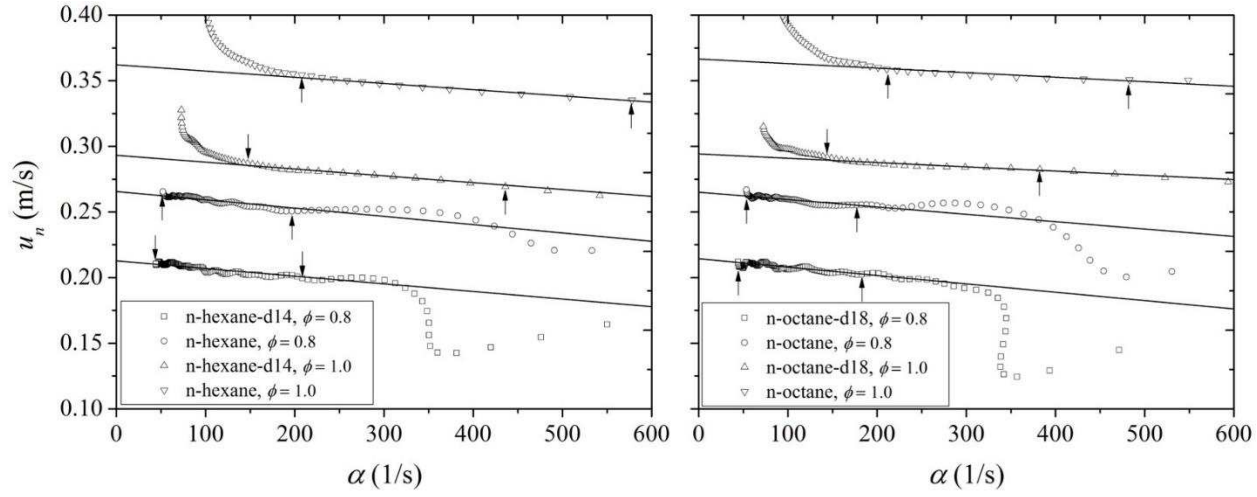

215

216 Figure 4 – Variation of stretched burning velocity, u_n, with stretch rate, α, for the normal and
217 deuterated alkanes at ϕ = 0.8 and 1.0. Vertical arrows indicate the data regions used for
218 application of laminar burn rate theory to obtain unstretched burning velocity and Markstein
219 lengths

220

Data for u_l, $u_{n,10mm}$ and $u_{n,30mm}$ are presented in tabulated form in Tables 1 for $\phi = 0.8$ and Table 2 for $\phi = 1.0$. The deuterated alkanes were found to burn approximately 20% slower than their normal alkane counterparts, a proportion that was independent of equivalence ratio, flame radius or whether the flame was unstretched or stretched.

	n-C_6H_{14} (m/s)	n-C_6D_{14} (m/s)	u_{C6D14} / u_{C6H14}	n-C_8H_{18} (m/s)	n-C_8D_{18} (m/s)	u_{C8D18} / u_{C6H18}
u_l	0.266 ± 0.001	0.214 ± 0.002	0.805	0.265 ± 0.001	0.214 ± 0.001	0.808
$u_{n,10mm}$	0.253 ± 0.002	0.202 ± 0.005	0.798	0.251 ± 0.007	0.198 ± 0.001	0.789
$u_{n,30mm}$	0.260 ± 0.001	0.212 ± 0.006	0.814	0.258 ± 0.002	0.208 ± 0.001	0.806

Table 1 – Measured average laminar burning velocities for normal and deuterated alkanes at $\phi = 0.8$, with $T_i = 360$ K and $P_i = 0.5$ MPa. Also included are the standard deviation of the measured values and the ratios of the measured burn rates of deuterated over normal alkanes.

	n-C_6H_{14} (m/s)	n-C_6D_{14} (m/s)	u_{C6D14} / u_{C6H14}	n-C_8H_{18} (m/s)	n-C_8D_{18} (m/s)	u_{C8D18} / u_{C6H18}
u_l	0.366 ± 0.005	0.292 ± 0.003	0.798	0.364 ± 0.003	0.294 ± 0.004	0.807
$u_{n,10mm}$	0.343 ± 0.005	0.274 ± 0.002	0.799	0.346 ± 0.005	0.281 ± 0.001	0.812
$u_{n,30mm}$	0.361 ± 0.001	0.288 ± 0.003	0.798	0.362 ± 0.003	0.293 ± 0.002	0.809

Table 2 – Measured average laminar burning velocities for normal and deuterated alkanes at $\phi = 1.0$, with $T_i = 360$ K and $P_i = 0.5$ MPa. Also included are the standard deviation of the measured values and the ratios of the measured burn rates of deuterated over normal alkanes.

The burned gas Markstein length, L_b, is a physico-chemical flame parameter used to characterise the effect of stretch rate on burn rate [35]. A small value of L_b is indicative of small influence of

flame stretch rate on burning velocity [26]. Burned gas Markstein lengths were determined as the slope of the linear fits in the u_n vs α plots (Figure 4). It should be noted that compared to the linear stretch corrections employed here, application of non-linear stretch corrections for the same data led to differences smaller than the experimental accuracy. Average L_b results for the conditions explored here are shown in Table 3 and demonstrate great similarity between the normal and deuterated alkanes, hence supporting the interpretation that the difference in burning velocity was independent of flame stretch (i.e. as shown in Tables 1 and 2). The similarity in L_b between the alkanes examined is likely to be due to their similar molar masses.

	n-C_6H_{12}, L_b (mm)	n-C_6D_{12}, L_b (mm)	n-C_8H_{16}, L_b (mm)	n-C_8D_{16}, L_b (mm)
$\phi = 0.8$	0.37 ± 0.020	0.37 ± 0.019	0.38 ± 0.049	0.39 ± 0.009
$\phi = 1.0$	0.33 ± 0.004	0.32 ± 0.012	0.27 ± 0.025	0.23 ± 0.044

Table 3 – Measured average Markstein lengths, L_b, for the normal and deuterated alkanes. Also included is the standard deviation between measurements performed at given equivalence ratios.

Normal versus deuterated alkanes have no differences in molecular structure and equilibrium calculations revealed negligible differences in adiabatic flame temperature, T_{ad}. Likewise, computations suggested very similar thermal and mass diffusion coefficients for these fuel-air mixtures (Table 4). The estimates displayed in Table 4 were based on the kinetic theory of gases developed by Chapman and Enskog and described in detail in [39], in conjunction with multi-component transport coefficients derived with the use of the equations defined in [40]. The thermodynamic data required for the calculations were provided by ExxonMobil [41]. Collision radii and reduced energies for the application of the kinetic theory of gases were estimated from

critical temperature and pressure data found in the NIST online library [42]. It may thus be concluded that since the values of thermal and mass diffusivity of the deuterated and normal alkane-air mixtures are virtually identical, the observed difference in burning velocities cannot be attributed to transport properties of the fuel molecule.

Temperature, T	$\frac{a_{C6D14-air}}{a_{C6H14-air}}$	$\frac{a_{C8D18-air}}{a_{C8H18-air}}$	$\frac{D_{C6D14-air}}{D_{C6H14-air}}$	$\frac{D_{C8D18-air}}{D_{C8H18-air}}$
360 K	0.995	0.997	0.973	0.977
$T = T_{ad} \approx 2350$ K	1.000	0.999	0.974	0.978

Table 4 – Ratios of thermal, α, and mass, D, diffusivities of deuterated versus normal alkane-air stoichiometric mixtures at 360 K and T = Tad, at constant pressure of 0.5 MPa.

To put the reduction of the laminar burning velocity of the deuterated alkanes relative to their respective hydrogen-containing counterparts in perspective, it was recently shown [6] that for identical conditions (T_i, P_i, ϕ), the unstretched burning velocity of the hexane isomer, 2,2 dimethyl butane, was measured to be 15% lower than that of n-hexane. This difference may be attributed to (i) the potential for the production of a higher proportion of CH_3 radicals during branched alkane combustion relative to those generated during n-alkane combustion, and (ii) the predominance of primary C-H bonds relative to the number of secondary C-H bonds in the n-alkane [4, 6]. Any causes of the 20% difference measured here between n-hexane and n-hexane-d14 pertaining to chemistry are limited to kinetic isotope effects of reaction rates involving H versus D atoms derived from the primary fuel molecule or contained in other combustion intermediates. However, a very important, supplementary factor which also affects laminar flame propagation is the lower diffusivity of D versus H atoms.

3.2 Turbulent Burning Velocities of the Alkanes

Turbulent tests were performed solely at $\phi = 1.0$ for a turbulent r.m.s. velocity of 4 m/s. Schlieren derived turbulent burn rates plotted against flame radius are shown in Figure 5. The reasoning behind setting 30 mm as the reference mean flame radius was explained at the beginning of Section 3. It was found that the deuterated fuels remained slower than their conventional counterparts under turbulence. However, the differences were substantially reduced compared to the laminar flames. Nevertheless, overall reductions throughout flame development subsequent to the spark affected region remained at 5-10% as a result of the substitution of H for D in both of the alkanes that were studied here. The average difference in burn rate between normal and deuterated alkanes at the reference radius of 30 mm was 8% (Figure 5).

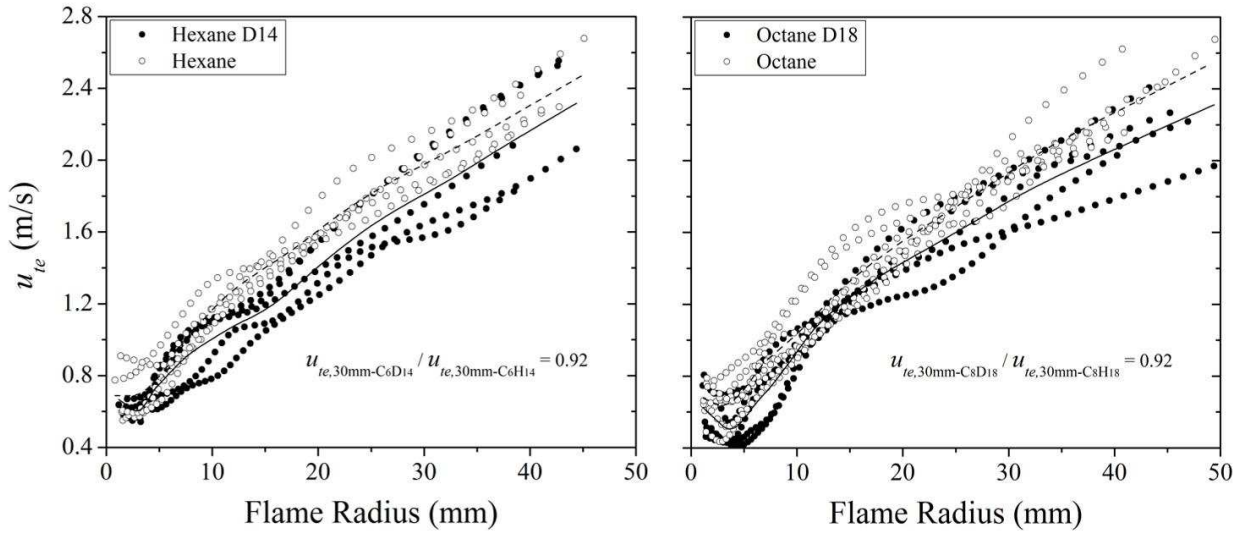

Figure 5 – Turbulent burning velocities (u' = 4 m/s) for the alkanes plotted against mean flame radius. The curves in the plots are averages at set radii obtained via linear interpolation; dashed lines for normal alkanes, solid lines for deuterated alkanes. Also shown are ratios of the normal vs. deuterated alkane at the reference radius of 30 mm.

A similar reduction of the differences between the burn rates of various hydrocarbon fuels when moving from laminar to turbulent conditions was reported in the previous paper [6] of the overall

study, which addressed the influence of molecular structure for a series of C_6 hydrocarbon fuels. As discussed in Section 3.1, the unstretched laminar burning velocity of 2,2 dimethyl butane has been found to be ~15% lower than that of n-hexane for near stoichiometric conditions, at 0.5 MPa and 360 K [6]. However, at the same equivalence ratio, pressure and temperature, the turbulent burning velocity of 2,2 dimethyl butane was only ~9% lower than that of n-hexane (at u' = 2 m/s and 6 m/s). Similarly [6], at the same equivalence ratio, pressure and temperature conditions, 2-methyl pentane was measured to have ~11% lower laminar burn rate than n-hexane, whereas its turbulent burn rate was found to be ~5% slower than that of n-hexane at u' = 2 m/s and 6 m/s. These observations indicate that there are residual kinetic and transport processes influencing turbulent combustion. In the case of the C_6 work reported in [6], the kinetic differences were primarily linked to the propensity of production of CH_3 vs C_2H_5 radicals during the initial steps of fuel oxidation and, consequently, the availability of H radicals and the facilitation of branching reactions at the flame front. Likewise, in the current work, the relative differences between the turbulent burn rate of the normal and deuterated alkanes studied here point to a specific contribution to turbulent flame propagation of the kinetics and transport processes involving H and D atoms and related radicals, such as OH / OD or HO_2 / DO_2.

Based on the turbulent regime theory [43], the alkane flames explored were classified as thickened flamelets, for which the Kolmogorov turbulent scale, η, is typically less than the laminar flame thickness, δ_l, and hence turbulence can penetrate the flame and alter the transport and chemistry of species at the flame front. In this case, application of the Zimont submodel for turbulent burning velocity [44], which has been extensively discussed elsewhere [45], is valid.

$$u_{te} \sim u'^{0.75} L^{0.25} u_l^{0.5} \alpha^{-0.25} \quad (1)$$

In this work, *u'*, the rms turbulent velocity, and L, the integral length scale of turbulence, remained constant for all flames. The reduced differences measured when moving from laminar to turbulent conditions were adequately replicated via application of Eq. (1). Utilising u_l and α data from Tables 2 and 4, it can be shown that the turbulent burn rate ratios of C_6D_{14} / C_6H_{14} and C_8D_{18} / C_8H_{18} predicted via Eq. (1) are 0.898 and 0.899, i.e. very similar to those experimentally measured at 0.9 – 0.95 throughout flame development within the vicinity of the bomb windows. Application of Eq. (1) for the C_6 hydrocarbon pairs can be shown to yield similarly good agreement between predictions and actual measurements. Therefore, it could be concluded that for fuels of similar molar mass, and consequently transport properties, the kinetic processes at the flame front only influence turbulent burning velocity indirectly, through the laminar burning velocity accordingly to Eq. (1).

3.3 Laminar Burning Velocities of H_2 and D_2

The development of the leanest and richest hydrogen-air and deuterium-air flames examined in the current study is illustrated via the filmstrips of schlieren images shown in Figure 6. These images have been zoomed in to better demonstrate the extremely early transition to cellular regime almost immediately following ignition (i.e. at r_u < 10 mm) for both fuels. To demonstrate the laminar flame development, shown in Figure 7 are plots of stretched laminar flame speed, u_n, versus flame radius for the leanest and richest deuterium and hydrogen flames examined.

The results for the stretched laminar burning velocities, u_n, at mean flame radii of r_u = 10 mm and 30 mm are displayed in Figure 8. It is important to clarify that these burning velocities do not reflect the pure, one-dimensional, unstretched laminar burning velocity (u_l). The reason is the extremely early transition of the H_2 and D_2 flames to a cellular regime, which made application of

342 the laminar flame theory to calculate u_l impossible [26]. Hence, in the case of the results of
343 Figure 8, diffusion effects are twofold, as they also include the increased diffusivity arising from
344 the increased surface area induced by cellularity. This effect is not expected to be identical
345 between H_2 and D_2 flames. The propensity to cellularity in fuel-air flames is believed to be
346 related to the Lewis number, $Le = \alpha_{mix} / D_{deficient\ reactant}$, of the deficient reactant [34].
347 Computations following the methods described in [39] and [40] showed that at $0.6 \leq \phi < 1.0$,
348 where fuel is the deficient reactant, Lewis numbers for H_2-air flames were 20-25% smaller than
349 those for D_2-air flames. Hence, instability effects are anticipated to be more prominent in H_2 than
350 in D_2 at $0.6 \leq \phi < 1.0$.

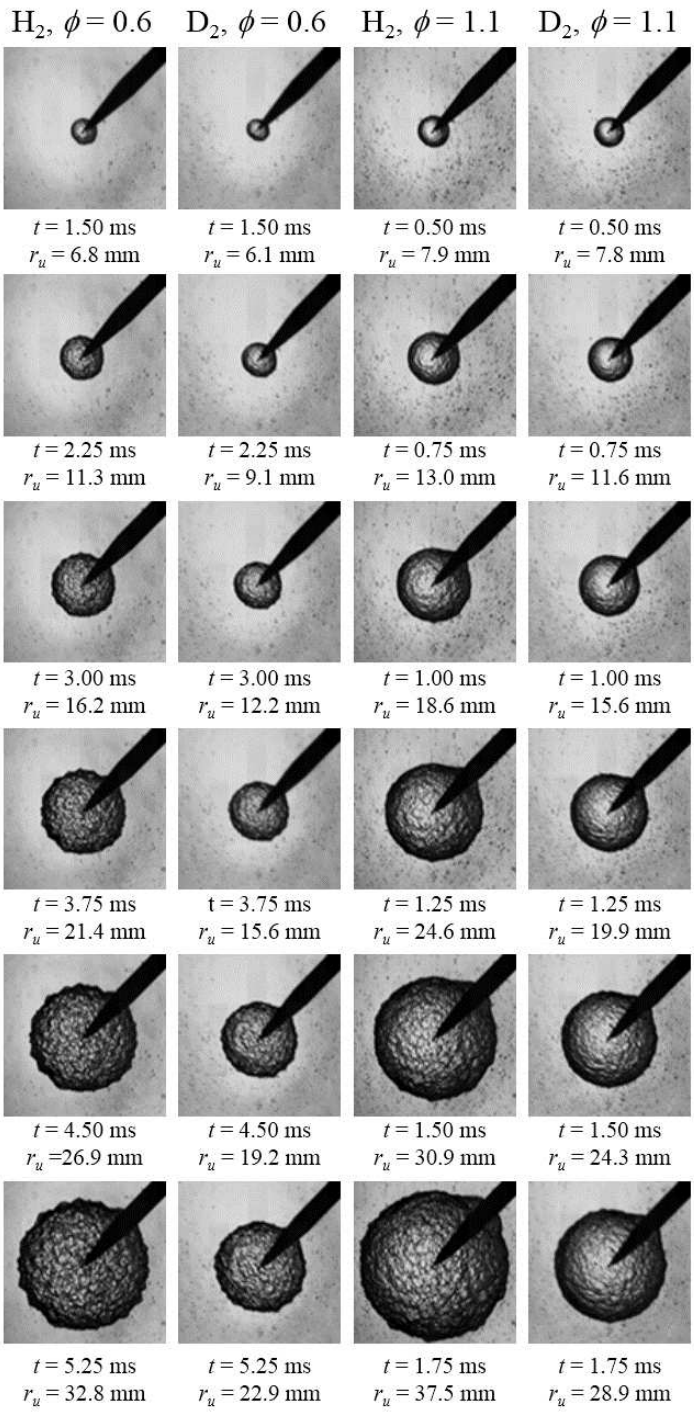

Figure 6 – Filmstrip (top to bottom) of schlieren images showing the flame development for hydrogen-air and deuterium-air flames at ϕ = 0.6 and ϕ = 1.1. The time values shown in ms represent time elapsed from the first visible flame kernel following ignition.

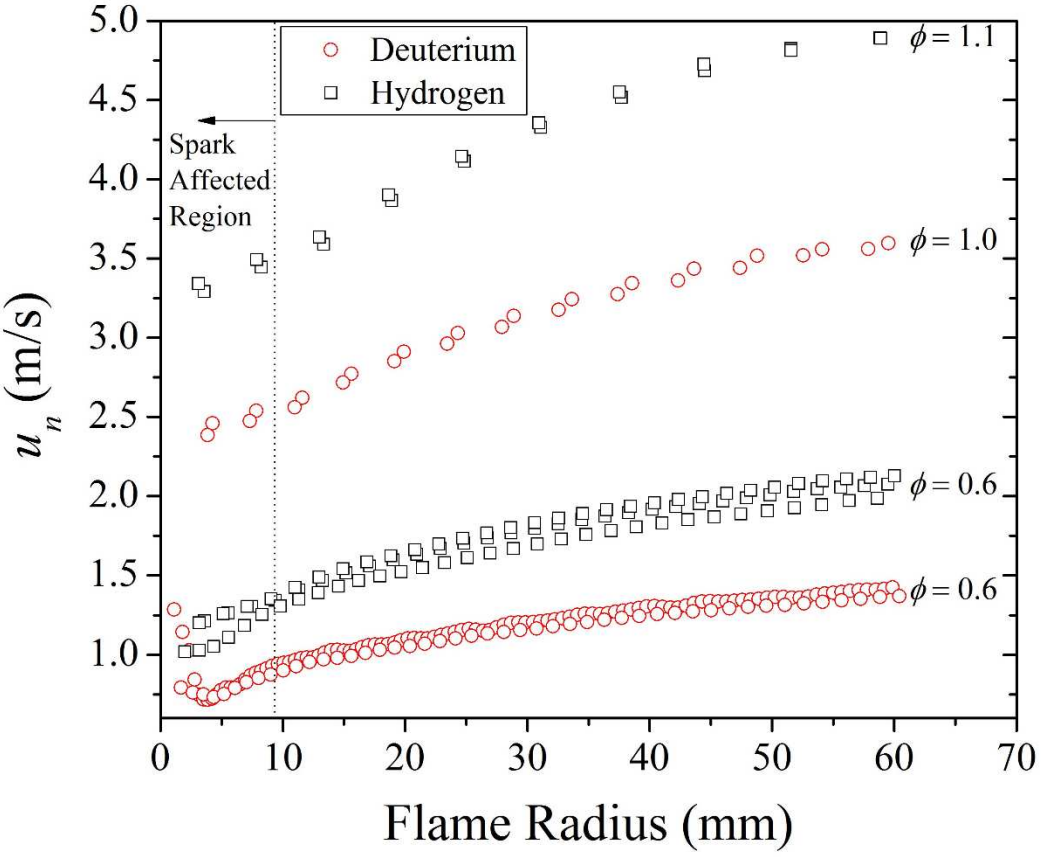

355

356 Figure 7 – Plots of stretched burning velocity versus flame radius showing the flame

357 development of the leanest and richest hydrogen and deuterium flames studied.

358

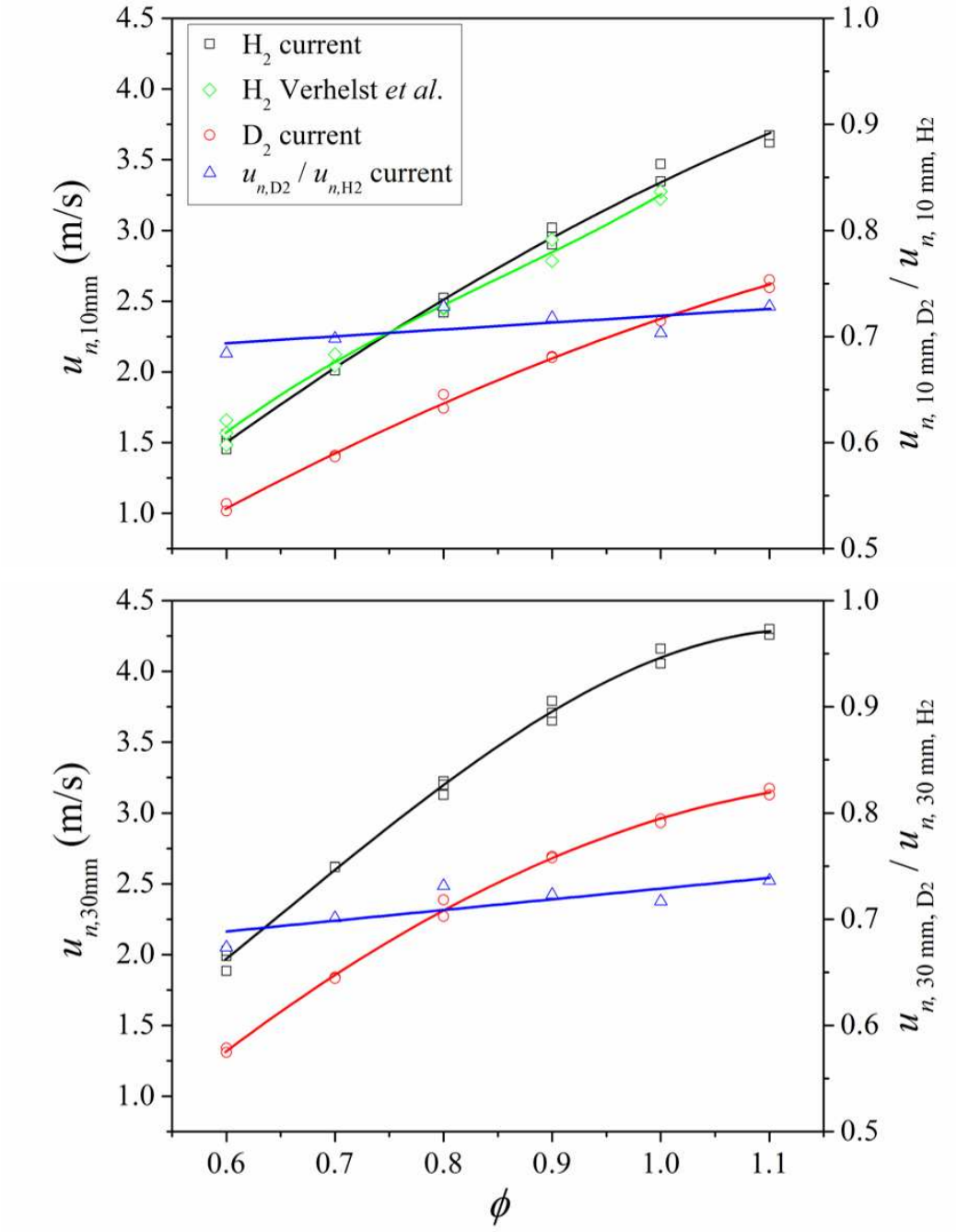

Figure 8 – Schlieren based laminar burn rates for H_2-air, D_2-air flames at mean flame radii of 10 mm and 30 mm, plotted versus ϕ. The curves are 3rd order polynomial fits of the experimental data. Also included in the plot for mean flame radius of 10 mm (top) are data for the burn rate of H_2 reported in [13] at identical conditions.

Focusing on the results of Figure 8, an increase in burn rate with ϕ was measured for both fuels over the range of ϕ explored. The ratio $u_{n,D2}$ / $u_{n,H2}$ varied from 0.69 ± 0.05 at ϕ = 0.6 to 0.73 ± 0.1 at ϕ = 1.1 for both flame radii assessed. These findings are almost identical to those reported in [19] for hydrogen and deuterium flames with oxygen, albeit this earlier paper did not indicate whether the flames were cellular.

Data reported in [13] for hydrogen-air mixtures are compared with the schlieren derived laminar burn rates for H_2-air reported here (Figure 8, top graph). The apparatus and initial conditions used in the two studies were identical. Differences in the burn rates ranged from ~ 1% at ϕ = 0.6 to a maximum of ~ 4% at ϕ = 1.0. These small discrepancies could be attributed to uncertainties in the equivalence ratio and slight differences in the imaging equipment and processing technique used. In another study of H_2 combustion performed in the Leeds MkII bomb [10], utilisation of a faster digital camera system enabled the determination of unstretched laminar burning velocities. Values of u_l reported in [10] were 30-40% lower compared to the $u_{n,10mm}$ values presented here, with the percentage difference becoming smaller with increasing ϕ. Given that there is a very early transition from laminar to cellular H_2 flames, and especially for lean flames, these differences could be attributed, primarily, to the effect of cellularity and, secondarily, to the effect of stretch rate.

To enable interpretation of the observed behaviour, computations for T_{ad} and transport coefficients were performed using the methods cited in Section 3.1 for the alkanes. In this case, any additional thermodynamic data required for the calculations was found in [46]. Although the overall predicted trend in T_{ad} vs ϕ was consistent with that for the laminar burn rate vs ϕ (cf. Figure 9a and Figure 8), the differences between the adiabatic flame temperature for H_2 and D_2 at a given equivalence ratio were too small to account for the measured differences in their laminar

burn rates. Also included in Figure 9 are computations for the ratios of thermal diffusivity of the mixtures, $\alpha_{D2\text{-air}}$ / $\alpha_{H2\text{-air}}$ (Fig. 9b), and effective mass diffusivities, D_{D2} / D_{H2} (Fig. 9c), and D_D / D_H (Fig. 9d), at the constant pressure (0.5 MPa) adiabatic flame temperature. Computed values for $\alpha_{D2\text{-air}}$ / $\alpha_{H2\text{-air}}$ ranged between 0.81 at ϕ = 0.6 and 0.75 at ϕ = 1.1. Values for the mass diffusivities were calculated to be D_{D2} / D_{H2} ~ 0.66 and D_D / D_H ~ 0.73 at all equivalence ratios explored. The ratios for D_{D2} / D_{H2} given here are consistent with that derived by Gray et al [20], for which D_{D2} / D_{H2}= 0.72 over a range of burnt gas compositions of $H_2 – O_2$ and $D_2 – O_2$ flames at low pressure. Based on a dependence of flame speed proportional to $\sqrt{D}$, they attributed a maximum decrease in flame speed in deuterium-containing mixtures to be 0.85 of that in hydrogen-containing mixtures. This is insufficient to account solely for the overall differences observed in the burning velocities.

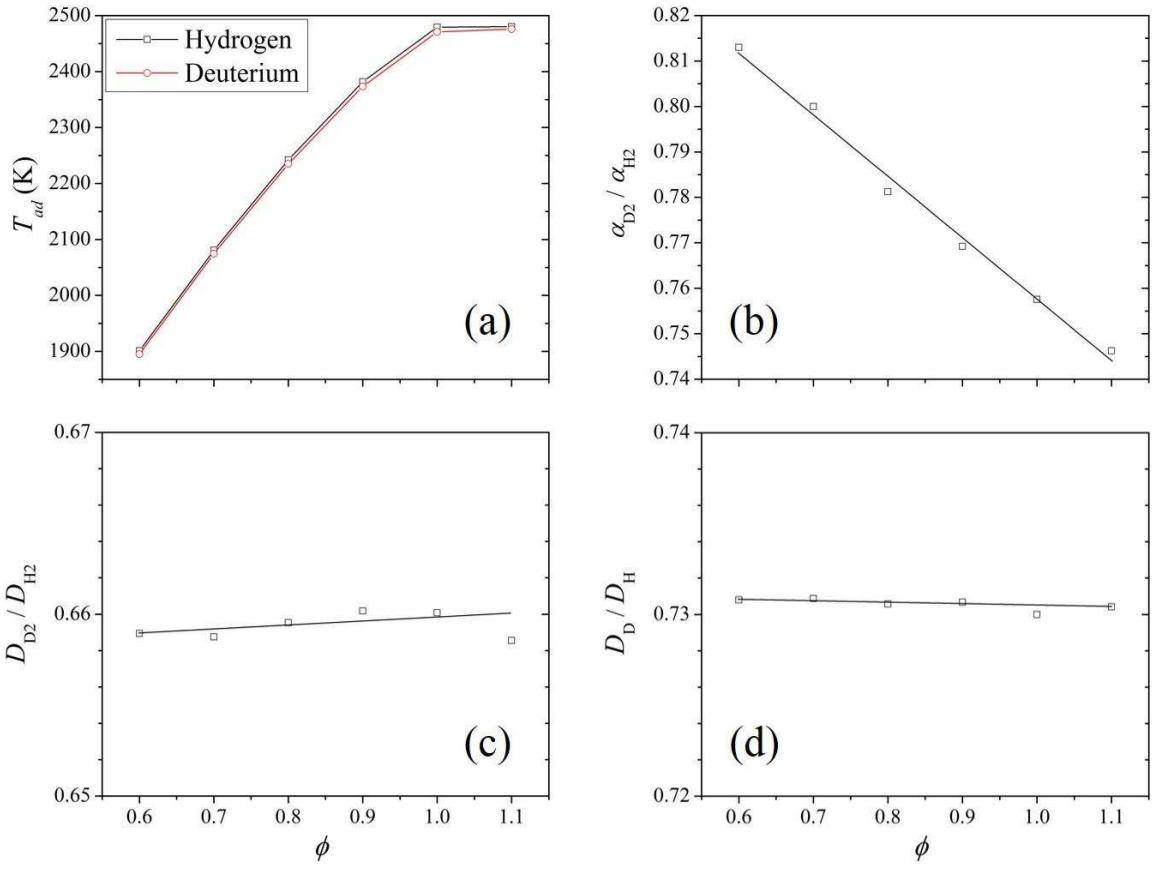

Figure 9 – Computed adiabatic temperatures for H_2-air, D_2-air flames for initial conditions of 360 K and 0.5 MPa. Also shown are ratios of thermal diffusivities of D_2 over H_2 and mass diffusivities of D_2 over H_2 and D over H calculated at the constant pressure (0.5 MPa) adiabatic flame temperature.

Numerous studies [e.g. 11, 47-48] have highlighted the critical importance of reactions R1 to R4 on controlling the burning velocity of H_2-air flames.

$$H + O_2 \Leftrightarrow OH + O \qquad (R1)$$

$$O + H_2 \Leftrightarrow OH + H \qquad (R2)$$

$$OH + H_2 \Leftrightarrow H_2O + H \qquad (R3)$$

$$H + O_2 + M \rightarrow HO_2 + M \qquad (R4)$$

The burn rate of the D_2 – air system is similarly controlled by the equivalent reactions. However, their rates will be susceptible to kinetic isotope effects, which must effect the corresponding rate constants. The ratios, k_D/k_H, for the forward Reactions R1 – R4 are displayed in Figure 10. Data were taken from references [20, 49]. The computations showed that the rate constants of D_2 were approximately 0.71, 0.62, 0.8 and 0.5 times those of H_2 for reactions R1, R2, R3 and R4, respectively. An analysis by Gray et al [20] attributed a geometric mean of the ratio of the rate constants (k_D/k_H) for reactions R1 – R3 at 2500K to be 0.59.

The dependence of the laminar burning velocity on the fundamental physical and kinetic parameters has been described as $u_n \sim (\alpha.\omega)^{0.5}$, where α is the thermal diffusivity of the mixture and ω is the global reaction rate [50]. This approximation is likely to be more valid for the relatively simple H_2-air and D_2-air combustion systems, than for those of hydrocarbon fuels. The laminar burn rate of deuterium could thus be estimated via,

$$u_{n,D2} \sim \left(\frac{(a.\omega)_{D2}}{(a.\omega)_{H2}} \right)^{0.5} .u_{n,H2} \qquad (2)$$

The reaction rate terms in Eq. (2) were set to be equal to the weighted average of the reaction rates of the critically important Reactions R1-R4. This weighted average was based on laminar burn rate sensitivity factors, S_i, reported in [11]. More specifically, to get the global reaction rate ratio of Eq. (2), the k_D/k_H ratios for reactions R1 – R4 (Figure 10) were multiplied by weighted laminar burn rate sensitivity factors, determined as $S_{i,w} = S_i / \Sigma S_i$. The values used for the thermal diffusivity ratio of equation 2 were those displayed in Figure 9b. The $u_{n,D2}$ values estimated via equation 2, combined with experimental $u_{n,H2}$ data, are shown in Figure 11. Agreement with the experimentally measured laminar burn rates of D_2-air flames is good. The difference ranged from ca. 12% at $\phi = 0.6$ to ca. 2% at $\phi = 1.1$. The over-prediction at lean mixtures could be attributed to the effects of cellularity, encapsulated in the experimentally determined $u_{n,H2}$ data used for the estimate. The reasoning behind this was described at the beginning of this section, with respect to the discussion of the results of Figure 8.

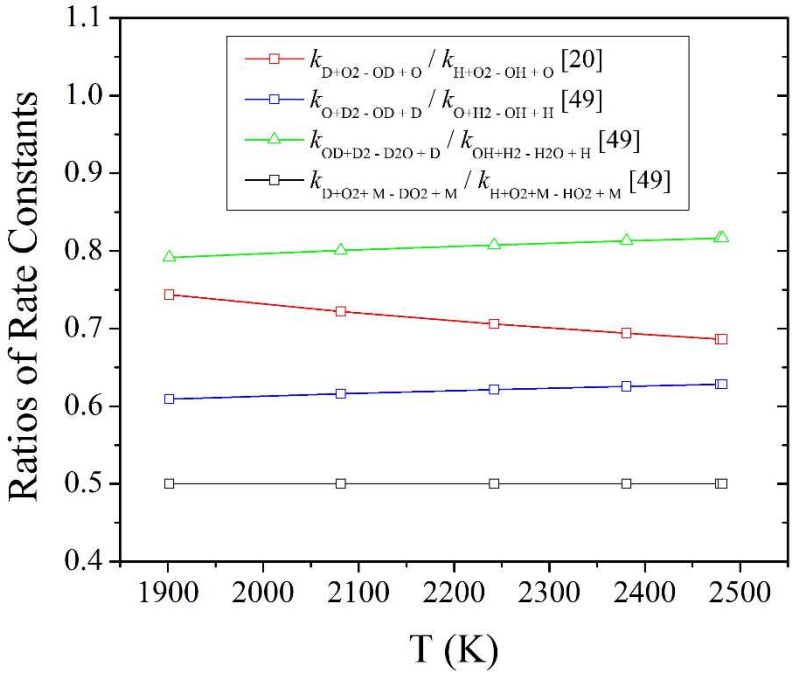

Figure 10 – Ratios of selected reaction rate constants, k_{D2} / k_{H2}, at temperatures relating to the T_{ad} at each of the equivalence ratios for which burn rates were experimentally measured.

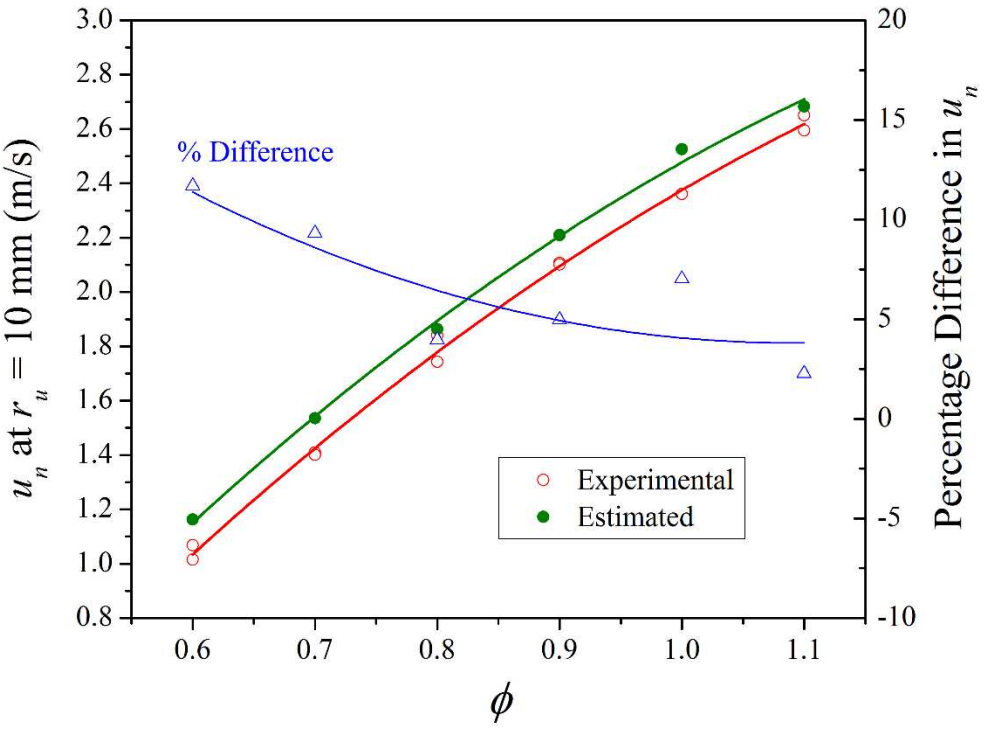

Figure 11 – Comparison between measured and estimated burn rates of D_2-air laminar flames at various equivalence ratios. The curves are 2nd order polynomial fits of the data, added for better illustration.

3.4 Turbulent Burning Velocities of H_2 and D_2 flames in air

For completeness, a filmstrip showing H_2-air and D_2-air flame images for the leanest and richest conditions explored in this study is included in Figure 12. For both fuels, lean flames appeared more distorted compared to rich flames. Schlieren derived turbulent burning velocities for H_2 and D_2 at mean flame radii of 30 mm and u' = 4 m/s, over the range ϕ = 0.6 to ϕ = 1.1, are displayed in Figure 13. To indicate the experimental scatter, also included in Figure 13 is the standard deviation from the average u_{te} values at each condition. The change from laminar to turbulent

conditions resulted in a significant reduction in the burn rate differences between H_2 and D_2. These differences fell from 25-30% under laminar conditions to ~ 5% when turbulence was present. This reduction was more marked than that for the normal vs deuterated alkanes, as discussed in Section 3.2.

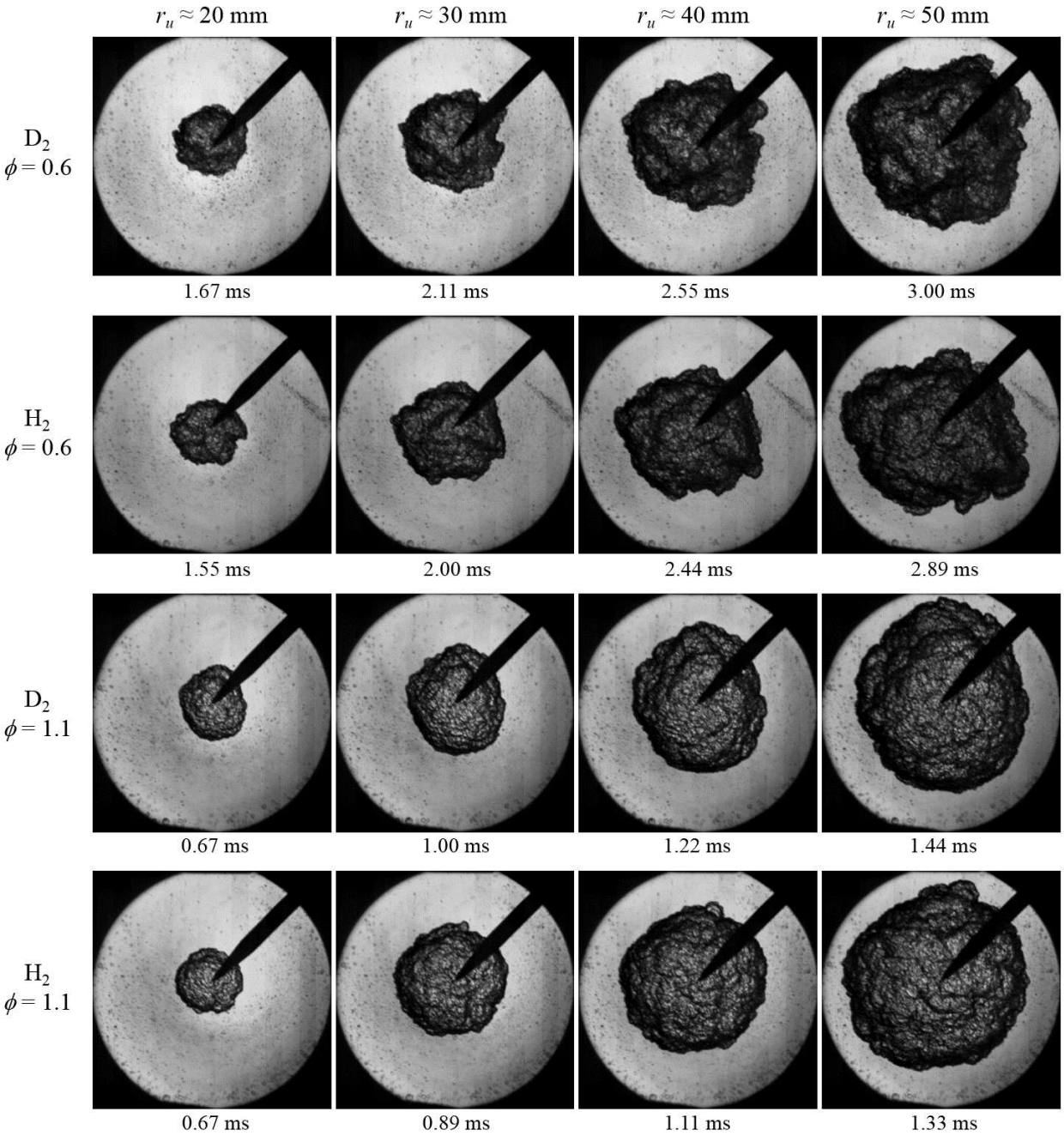

Figure 12 – Filmstrips of turbulent flame images for H_2 and D_2 at equivalence ratios of 0.6 and 1.1. The mean flame radius values indicated have minimum accuracy of ± 1.0 mm.

Although a general trend to lower turbulent burning velocities of D_2 flames relative to those of H_2 is evident in Figure 12, the individual results tend to overlap within the range of experimental scatter. The similarity between the turbulent burning velocities of deuterium and hydrogen flames, contrasted with the marked difference of their laminar burning velocities, suggests that turbulent transport processes have a greater influence on the flame propagation rate than kinetic isotope effects involved in the kinetic chain branching reactions.

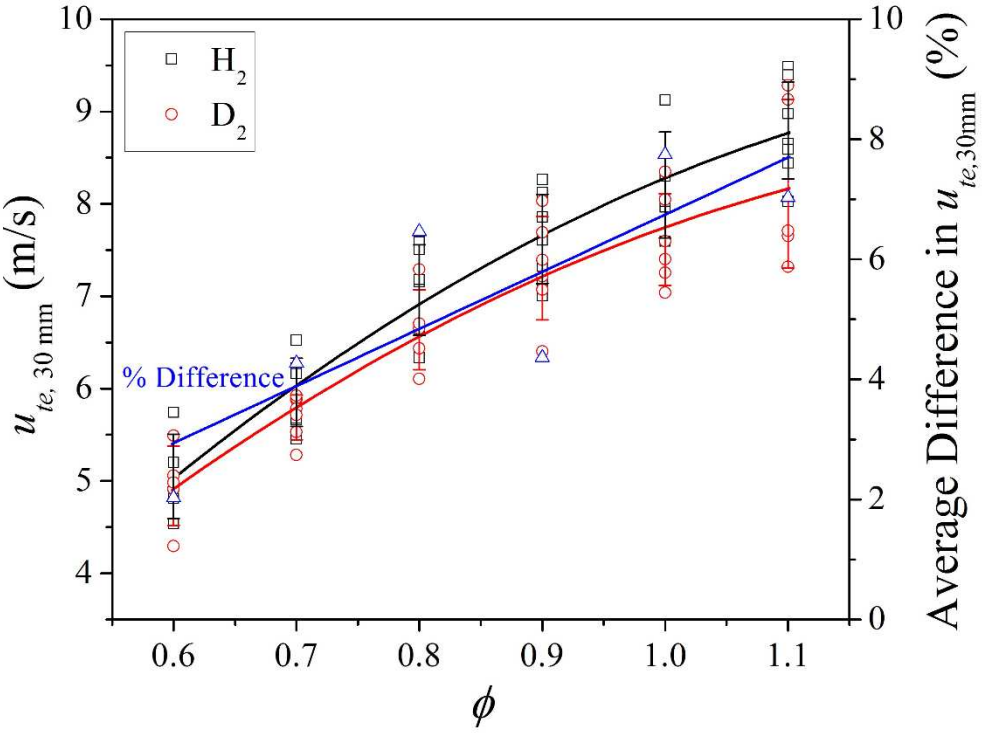

Figure 13 – Schlieren based turbulent burning velocities (u' = 4 m/s) for hydrogen and deuterium at a mean flame radius of 30 mm. The standard deviation from average experimental data at each condition along with the average percentage difference between the two fuels are also shown.

Application of Eq. (1) for the H_2 and D_2 flames examined is not as straightforward as for the normal and deuterated alkanes. First, for reasons discussed earlier in Section 3.3, the analysis for the H_2 and D_2 laminar flames could not yield a true unstretched laminar burning velocity, as required for appropriate application of Eq. (1). Second, owing to their very high laminar burn rate and small flame thickness, the H_2 and D_2 turbulent flames examined are classified as corrugated flames, in which case the condition of $\eta << \delta_l$ does not necessarily stand. Nonetheless, estimations made through Eq. (1) still are in fair agreement with the experiments. Estimations from Eq. (1) for the u_{te} ratio between D_2 and H_2 ranged from 0.88 at lean conditions to 0.94 at rich conditions.

4. Conclusions

Substitution of the hydrogen atoms in n-hexane and n-octane with deuterium atoms resulted in a reduction of ca. 20% in the measured laminar burning velocity, despite there being little difference in molar mass or calculated adiabatic flame temperatures, and no expectation of qualitative differences in the kinetic scheme for full oxidation of the normal and deuterated alkane counterparts. Also, it was assumed that the kinetic scheme for full oxidation of the normal and deuterated alkane counterparts were the same. The normal alkane flames were observed to become cellular slightly earlier. Nonetheless, insofar that comparisons were made with respect to the unstretched burning velocities calculated using data corresponding to the pre-cellular region of the flame, instability effects cannot be considered to be significant. It is concluded that the observed difference in laminar burn rates between normal and deuterated n-hexane and n-octane are the result, predominantly, of the higher thermo-diffusivity and reactivity of hydrogen atoms relative to those of deuterium atoms.

Measured laminar burn rates for H_2-air flames were 30% higher than for D_2-air flames, at fixed ambient temperature, pressure and equivalence ratios. This difference was also linked to the thermo-diffusive and chemical kinetic properties of H vs D atoms. The ratios of thermal and mass diffusivity of deuterium over hydrogen atoms, as well as corresponding reaction rate ratios for the important chain branching reactions involving D and H, were estimated to be within 0.6 – 0.8 over the range of conditions explored, which is very similar to the measured difference in laminar burn rate. The higher laminar burn rate difference between H_2 and D_2 compared with that measured for normal versus deuterated alkanes would be expected, in view of the kinetic complexity and weakened isotope effect in the hydrocarbon combustion chemistry.

Under turbulent conditions, differences in the burn rate between normal and deuterated n-hexane and n-octane were much smaller, with the deuterated alkanes being ~8% slower than their normal counterparts. It is concluded that turbulence globally accelerates species diffusivity, rendering transport properties of species within the preheat zone more important for turbulent compared to laminar flames. Given that the thermal diffusivity of the parent fuels is almost identical between the normal and deuterated alkane counterparts, the residual influence of kinetic isotope effects is expressed as $u_l^{0.5}$.

The difference between the burn rates of H_2-air flames and D_2-air flames under turbulence was reduced by a factor of five relative to that observed under laminar conditions. These findings emphasise that transport properties, globally boosted by turbulent diffusivity, exert greater control than kinetic isotope effects during turbulent combustion. The measured turbulent burning velocity ratios at each mixture stoichiometry examined were adequately replicated via application of the Zimont submodel for turbulent burning velocity, defined in Eq. (1).

Acknowledgements

The support of Exxon Mobil and Mercedes-Benz High Performance Engines is gratefully acknowledged.

References

[1] Gu, X., Huang, Z., Wu, S., "Laminar burning velocities and flame instabilities of butanol isomers–air mixtures", Combust Flame 157: 2318-2325 (2010)

[2] Wu, F., Kelley, A.P., Law, C.K., "Laminar flame speeds of cyclohexane and mono-alkylated cyclohexanes at elevated pressures", Combust Flame 159: 1417-1425 (2012)

[3] Mehl, M., Herbinet, O., Dirrenberger, P., Bounaceur, R., Glaude, P.A., Battin-Leclerc, F., Pitz, W.J., "Experimental and modeling study of burning velocities for alkyl aromatic components relevant to diesel fuels", Proc Combust Inst 35: 341-348 (2015)

[4] Farrell, J.T., Johnston, R.J., Androulakis, I.P., "Molecular Structure Effects on Laminar Burning Velocities at Elevated Temperature and Pressure", SAE Tech Paper 2004-01-2936 (2004)

[5] Beeckmann, J., Cai, L., Pitsch, H., "Experimental investigation of the laminar burning velocities of methanol, ethanol, n-propanol and n-butanol at high pressure", Fuel 117: 340-350 (2014)

[6] Burluka, A.A., Gaughan, R.G., Griffiths, J.F., Mandilas, C., Sheppard, C.G.W., Woolley, R., "Turbulent burning rates of gasoline components, Part 1 – Effect of fuel structure of C6 hydrocarbons", Fuel 167: 347-356 (2016)

[7] Burluka, A.A., Gaughan, R.G., Griffiths, J.F., Mandilas, C., Sheppard, C.G.W., Woolley, R., “Turbulent burning rates of gasoline components, Part 2 – Effect of carbon number”, Fuel 167: 357-365 (2015)

[8] Friedman, R., Burke, E., “Burning Velocities. Acetylene and Dideutero-Acetylene with Air”, Ind Eng Chem 43: 2772-2776 (1951)

[9] Buttini, P., Corno, C., Latella, A., Prastaro, M., "Relevance of adding deuterated hydrocarbons to fuels in the autovehicular emissions studies", SAE Paper 982622, 1998

[10] Bradley, D., Lawes, M., Liu, K., Verhelst, S., Woolley, R., “Laminar burning velocities of lean hydrogen–air mixtures at pressures up to 1.0 MPa”, Combust Flame 149: 162-172 (2007)

[11] Hu, E., Huang, Z., He, J., Miao, H., “Experimental and numerical study on laminar burning velocities and flame instabilities of hydrogen-air mixtures at elevated pressures and temperatures”, Int J Hydrogen Energ 34: 8741-8755 (2009)

[12] Pareja, J., Burbano, H.J., Amell, A., Carvajal, J., “Laminar burning velocities and flame stability analysis of hydrogen/air premixed flames at low pressure” Int J Hydrogen Energ 36: 6317-6324 (2011)

[13] Verhelst, S., Woolley, R., Lawes, M., Sierens, R., “Laminar and Unstable Burning Velocities and Markstein Lengths of Hydrogen–Air Mixtures at Engine-Like Conditions”, Proc Combust Inst, 30: 209-216 (2005)

[14] Zamashchikov, V.V., Alekseev, V.A., Konnov, A.A., “Laminar burning velocities of rich near-limiting flames of hydrogen”, Int J Hydrogen Energ 39: 1874-1881 (2014)

[15] Dahoe, A.E., “Laminar burning velocities of hydrogen–air mixtures from closed vessel gas explosions”, Journal of Loss Prevention in the Process Industries, 18: 152-166 (2005)

[16] Kido, H., Nakahara, M., Nakashima, K., and Kim, J., "Turbulent Burning Velocity of Lean Hydrogen Mixtures", SAE Technical Paper 2003-01-1773 (2003)

[17] Kitagawa, T., Nakahara, T., Maruyana, K., Kado, K., Hayakawa, A., Kobyashi, S., "Turbulent burning velocity of hydrogen–air premixed propagating flames at elevated pressures", Int J Hydrogen Energ 33: 5842-5849 (2008)

[18] Amato, A., Day, M., Cheng, R.K., Bell, J., Dasgupta, D., Lieuwen, T., "Topology and burning rates of turbulent, lean, H2/air flames", Combust Flame 162: (2015) 4553-4565

[19] Gray, P., Smith, D.B., "Isotope effects on flame speeds for hydrogen and deuterium", Chem Commun (London) 146-148 (1967)

[20] Gray, P., Holland, S., Smith, D.B., "The effect of isotopic substitution on the flame speeds of hydrogen-oxygen and hydrogen-nitrous oxide flames", Combust Flame 14: 361-374 (1970)

[21] Koroll, G.W., Kumar, R.K., "Isotope effects on the combustion properties of deuterium and hydrogen, Combust Flame 84: 154-159 (1991)

[22] Gillespie, L., Lawes, M., Sheppard, G.G.W., Woolley, R., "Aspects of Laminar and Turbulent Burning Velocity Relevant to SI Engines", SAE Tech Paper 2000-01-0192 (2000)

[23] Heywood, J.B., "Internal Combustion Engine Fundamentals, International Edition", Mc Graw Hill, ISBN 0071004998 (1988)

[24] Mandilas, C., "Laminar and Turbulent Burning Characteristics of Hydrocarbon Fuels", PhD Thesis, University of Leeds (2008)

[25] Bradley, D., Gaskel, P.H., Gu, X.J., "Burning Velocities, Markstein Length, and Flame Quenching for Spherical Methane-Air Flames: A Computational Study", Combust Flame 104: 176-198 (1996)

[26] Bradley, D., Hicks, R.A., Lawes, M., Sheppard, C.G.W., Woolley, R., "The Measurement of Laminar Burning Velocities and Markstein Numbers for Iso-octane–Air and Iso-octane–n-Heptane–Air Mixtures at Elevated Temperatures and Pressures in an Explosion Bomb", Combust Flame 115: 126-144 (1998)

[27] Lamoureux, N., Djebaili-Chaumeix, N., Paillard, C.E., "Laminar flame velocity determination for H2–air–He–CO2 mixtures using the spherical bomb method", 2nd Mediterranean Comb Symp, Exp Therm Fluid Sci 27: 385-393 (2003)

[28] Jerzembeck, S., Peters, N., "Laminar Spherical Flame Kernel Investigation of Very Rich Premixed Hydrocarbon-Air Mixtures in a Closed Vessel under Microgravity Conditions", SAE Tech Paper 2008-01-0471 (2008)

[29] Chen, Z., Wei, L., Huang, Z., Miao, H., Wang, X., Jiang, D., "Measurement of Laminar Burning Velocities of Dimethyl Ether−Air Premixed Mixtures with N2 and CO2 Dilution", Energ Fuels, 23: 735-739 (2009)

[30] Varea, E., Modica, V., Vandel, A., Renou, B., "Measurement of laminar burning velocity and Markstein length relative to fresh gases using a new post-processing procedure. Application to laminar spherical flames for methane, ethanol and isooctane/air mixtures", Combust Flame 159: 577-590 (2012)

[31] Moghaddas, A., Eisazadeh-Far, K., Metghalchi, H., "Laminar burning speed measurement of premixed n-decane/air mixtures using spherically expanding flames at high temperatures and pressures", Combust Flame 159: 1437-1443 (2012)

[32] Lawes, M., Ormsby, M.P., Sheppard, C.G.W., Woolley, R., "Variation of Turbulent Burning Rate of Methane, Methanol and Isooctane Air Mixtures with Equivalence Ratio at Elevated Pressure", Combust Sci Technol 177: 1273-1289 (2005)

[33] Abdi Aghdam, E., Burluka, A.A., Hattrell, T., Liu, K., Sheppard, C.G.W., Neumeister, J. and Crundwell, N., "Study of Cyclic Variation in an SI Engine using Quasi-Dimensional Combustion Model", SAE Paper 2007-01-0939 (2007)

[34] Law, C.K., "Dynamics of Stretched Flames", 22nd Symp Int Combust 22: 1381-1402 (1988)

[35] Bradley, D., Sheppard, C.G.W., Woolley, R., Greenhalgh, D.A., Lockett, R.D., "The development and structure of flame instabilities and cellularity at low Markstein numbers in explosions", Combust Flame 122: 195-209 (2000)

[36] Bradley, D., Lung, F.K., Spark ignition and the early stages of turbulent flame propagation, Combust Flame 69: 71-93 (1987)

[37] Abdel-Gayed, R.G., Bradley, D., Lawes, M., "Turbulent burning velocities: a general correlation in terms of straining rates", Proc R Soc Lond A414: 389-413 (1987)

[38] Jomaas, G., Law, C.K., Bechtold, J.K., On transition to cellularity in expanding spherical flames, J Fluid Mech, 583: 1-26 (2007)

[39] Bird, R.B., Stewart, W.E., Lightfoot, E.N., "Transport Phenomena, 2nd Edition", Wiley & Sons, ISBN 0471410772 (2002)

[40] Wilke, C.R., "A viscosity equation for gas mixtures", J Chem Phys 18: 517-519 (1950)

[41] Gaughan, R., Private Communication, University of Leeds (2008)

[42] http://webbook.nist.gov/chemistry/, accessed 05/2016

[43] Borghi, R., "Turbulent combustion modeling", Prog Ener Comb 14: 245-292 (1988)

[44] Zimont, V.L. “To computations of turbulent combustion of partially premixed gases, chemical physics of combustion and explosion processes. Combustion of multi-phase and gas systems”, OIKhF, Chernogolovka (1977) p. 77–80 (in Russian)

[45] Lipatnikov, A.N., Chomiak, J., “Turbulent flame speed and thickness: phenomenology, evaluation, and application in multi-dimensional simulations”, Prog Energ Comb Sci, 28: 1-74 (2002)

[46] http://garfield.chem.elte.hu/Burcat/burcat.html, accessed 05/2016

[47] Marinov, N.M., Curran, H.J., Pitz, W.J., Westbrook, C.K., “Chemical Kinetic Modeling of Hydrogen under Conditions Found in Internal Combustion Engines”, Energ Fuels 12: 78–82 (1998)

[48] Dong,Y., Holley, A.T., Andac, M.G., Egolfopoulos, F.N., Davis, S.G., Middha, P., Wang, H., “Extinction of premixed H2/air flames: Chemical kinetics and molecular diffusion effects”, Combust Flame 142: 374-387 (2005)

[49] Pamidimukkala, K.M., Skinner, G.B., “Resonance absorption measurements of atom concentrations in reacting gas mixtures. VIII. Rate constants for O+H2→OH+H and O+D2→OD+D from measurements of O atoms in oxidation of H2 and D2 by N2O”, J. Chem Phys 76: 311-315 (1982)

[50] Glassman, I., “Combustion, 3rd Edition”, Academic Press, ISBN 0122858522 (1996)